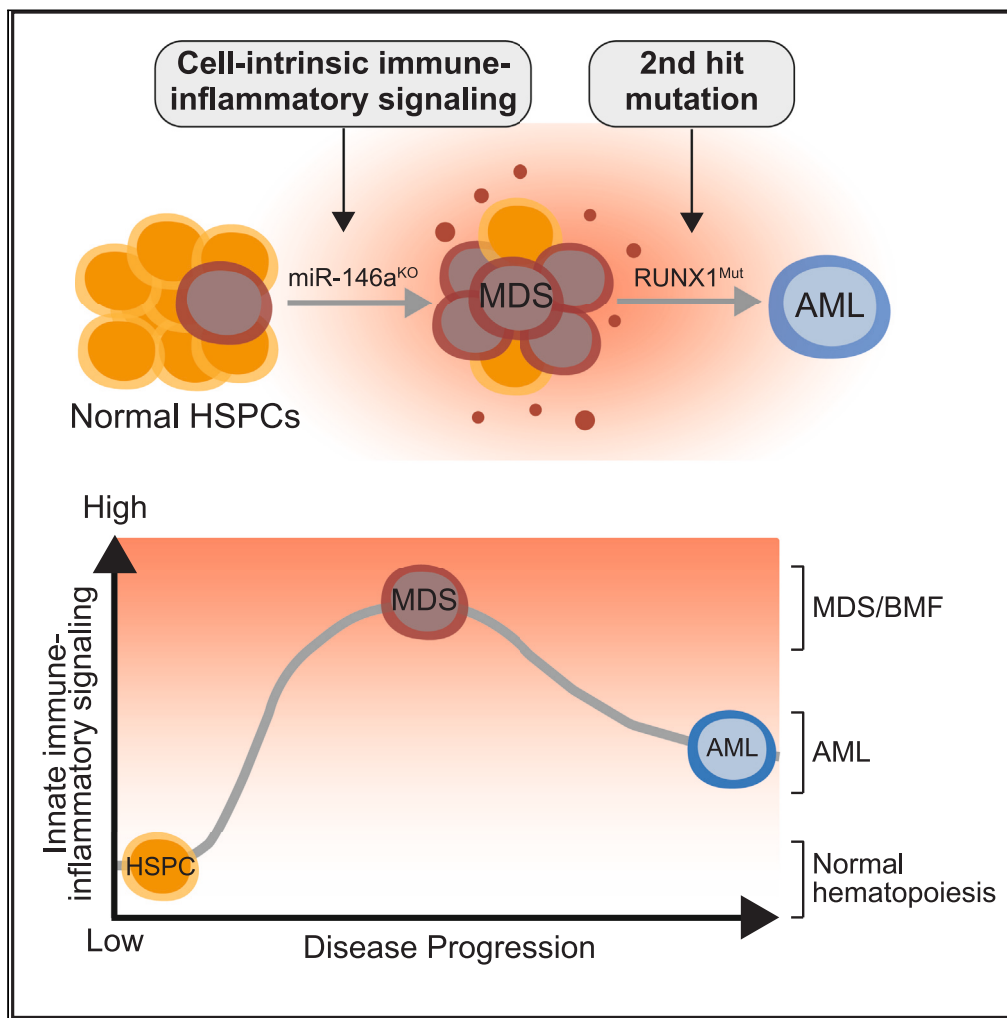## Article

Dysregulated innate immune signaling cooperates with RUNX1 mutations to transform an MDS-like disease to AML

Laura Barreyro,
Avery M. Sampson,
Kathleen Hueneman, ...,
Kenneth D. Greis,
Gang Huang,
Daniel T.
Starczynowski

daniel.starczynowski@cchmc.
org

Highlights

Deletion of miR-146a and the presence of RUNX1[mut] lead to MDS/BMF

HSPCs lacking miR-146a but with RUNX1[mut] progress to AML

RUNX1[mut] alters immune-inflammatory signaling and expands miR-146a[KO] HSPCs

miR-146a[KO]/RUNX1[mut] AML relies on immune-inflammatory signaling

Article

Dysregulated innate immune signaling cooperates with RUNX1 mutations to transform an MDS-like disease to AML

Laura Barreyro,[1] Avery M. Sampson,[1] Kathleen Hueneman,[1] Kwangmin Choi,[1] Susanne Christie,[1] Vighnesh Ramesh,[1] Michael Wyder,[2] Dehua Wang,[3,4] Mario Pujato,[5] Kenneth D. Greis,[2] Gang Huang,[1,6,7] and Daniel T. Starczynowski[1,2,8,9,*]

SUMMARY

Dysregulated innate immune signaling is linked to preleukemic conditions and myeloid malignancies. However, it is unknown whether sustained innate immune signaling contributes to malignant transformation. Here we show that cell-intrinsic innate immune signaling driven by miR-146a deletion (miR-146a^{KO}), a commonly deleted gene in myelodysplastic syndromes (MDS) and acute myeloid leukemia (AML), cooperates with mutant RUNX1 (RUNX1^{mut}) to initially induce marrow failure and features of MDS. However, miR-146a^{KO} hematopoietic stem and/or progenitor cells (HSPCs) expressing RUNX1^{mut} eventually progress to a fatal AML. miR-146a^{KO} HSPCs exhaust during serial transplantation, while expression of RUNX1^{mut} restored their hematopoietic cell function. Thus, HSPCs exhibiting dysregulated innate immune signaling require a second hit to develop AML. Inhibiting the dysregulated innate immune pathways with a TRAF6-UBE2N inhibitor suppressed leukemic miR-146a^{KO}/RUNX1^{mut} HSPCs, highlighting the necessity of TRAF6-dependent cell-intrinsic innate immune signaling in initiating and maintaining AML. These findings underscore the critical role of dysregulated cell-intrinsic innate immune signaling in driving preleukemic cells toward AML progression.

INTRODUCTION

Acute myeloid leukemia (AML) is an aggressive myeloid malignancy that arises in hematopoietic stem and/or progenitor cells (HSPCs). In some cases, AML can be preceded by preleukemic states, such as myelodysplastic syndromes (MDS).[1] The transition from MDS to AML typically involves the acquisition of mutations in genes like RUNX1, NRAS/KRAS, or FLT3.[2] However, the preleukemic molecular and cellular states that are amenable to transformation to overt AML are not entirely understood. In preleukemic conditions, there is a notable presence of cell-intrinsic innate immune signaling within mutant HSPCs. Additionally, dysregulated innate immune and inflammatory signaling can provide a competitive fitness advantage to mutant HSPCs, especially in the context of systemic inflammation, potentially leading to bone marrow failure (BMF) or MDS-like phenotypes.[3–6]

Although the dysregulation of cell-intrinsic innate immune signaling and chronic inflammation may contribute to the development of leukemia, it has not been definitively established whether they directly lead to AML or result in overt disease in mouse models. Nonetheless, mouse models featuring dysregulated cell-intrinsic innate immune signaling emphasize the significance of these pathways in hematologic malignancies.[3] For example, miR-146a, a commonly deleted gene in MDS and AML, negatively regulates the expression of several genes of the innate immune signaling, such as tumor necrosis factor (TNF) receptor-associated factor 6 (TRAF6) and interleukin 1 receptor-associated kinase 1 (IRAK1).[7–17] HSPCs from mice lacking miR-146a display constitutive activation of NF-κB via TRAF6 and IRAK1, contributing to ineffective hematopoiesis and BMF, although not resulting in AML.[18,19] Therefore, acquired mutations in HSPCs with dysregulated innate immune and inflammatory signaling are seemingly required for transformation into AML.

RUNX1 is one of the most frequently mutated genes in AML pathogenesis, undergoing various chromosomal translocations, loss-of-function mutations, and copy number gains.[20,21] Furthermore, RUNX1 mutations are linked to altered innate immune and inflammatory signaling

[1]Division of Experimental Hematology and Cancer Biology, Cincinnati Children's Hospital, Cincinnati, OH, USA
[2]Department of Cancer Biology, University of Cincinnati, Cincinnati, OH, USA
[3]Department of Pathology & Laboratory Medicine, University of Cincinnati, Cincinnati, OH, USA
[4]Department of Pathology, Cincinnati Children's Hospital, Cincinnati, OH, USA
[5]Life Sciences Computational Services, LLC, Huntingdon Valley, PA, USA
[6]Department of Cell Systems & Anatomy, UT Health San Antonio, San Antonio, TX, USA
[7]Department of Pathology & Laboratory Medicine, UT Health San Antonio, San Antonio, TX, USA
[8]University of Cincinnati Cancer Center, Cincinnati, OH, USA
[9]Lead contact
*Correspondence: daniel.starczynowski@cchmc.org
https://doi.org/10.1016/j.isci.2024.109809

and often act as secondary hits in the progression from MDS to AML.[22–24] Therefore, our study aimed to investigate whether RUNX1 mutations could lead to the development of overt AML in preleukemic cells displaying cell-intrinsic innate immune activation.

Here we show that cell-intrinsic innate immune and inflammatory signaling driven by deletion of the microRNA miR146a cooperates with a RUNX1 mutant to initially induce features of marrow failure. However, over time miR-146a-deficient (miR-146a^{KO}) HSPCs expressing mutant RUNX1 (RUNX1^{mut}) developed AML, which was not observed in mice engrafted with either miR-146a^{KO} or RUNX1^{mut} HSPCs. Moreover, expression of RUNX1^{mut} rescued the hematopoietic repopulation deficiency of miR-146a^{KO} HSPCs. Thus, HSPCs exhibiting dysregulated cell-intrinsic innate immune and inflammatory signaling require a second hit to develop AML. Gene expression analyses confirmed that deletion of miR-146a results in broad dysregulation of innate immune and inflammatory pathways; however, we observed that expression of RUNX1^{mut} in miR-146a^{KO} HSPCs unexpectedly restricted the expression of these pathways to discrete innate immune and inflammatory genes at the AML stage. Lastly, we show that inhibition of innate immune signaling with a TRAF6-UBE2N inhibitor was sufficient to suppress the leukemic miR-146a^{KO}/RUNX1^{mut} HSPCs, indicating that TRAF6-dependent cell-intrinsic innate immune signaling is not only required for initiating AML but is also necessary for sustaining the leukemic phenotype. Taken together, our findings revealed that dysregulation of cell-intrinsic innate immune signaling is required for propagating preleukemic cells and contributes to the progression of AML.

RESULTS

Loss of miR-146a and expression of RUNX1 mutant cooperate to induce an MDS/BMF-like disease

Since dysregulated innate immune and inflammatory signaling is observed in preleukemic states, it is viewed as an early alteration, while second-hit mutations, such as in RUNX1, RAS, or FLT3, are associated with malignant transformation.[2] Therefore, to model the progression from preleukemic states to overt AML, we introduced a dominant-negative RUNX1 frameshift mutant (S291fsX300, herein RUNX1^{mut}) into miR-146a knockout (KO) HSPCs.[25] This mutation results in the C-terminal truncation of the wild-type RUNX1 protein, which still retains DNA binding activity, but it is unable to recruit co-activators/repressors due to the lack of the transactivation domain.[26,27] Retroviral vectors (MSCV-IRES-GFP) encoding RUNX1^{mut} or an empty control were retrovirally transduced into CD45.2 wild-type C57BL/6J (WT) or miR-146a^{KO} bone marrow (BM) cells (Figure 1A). Expression of the transduced human RUNX1^{mut} and of miR-146a in BM cells was confirmed by quantitative PCR analysis (Figure S1A). The transduced GFP-expressing cells successfully engrafted and established chimerism in peripheral blood (PB) (Figure 1B). The majority of recipient mice transplanted with miR-146a^{KO}/RUNX1^{mut} BM cells (n = 10/15) succumbed to a hematologic malignancy within 14 months post-transplantation. Within the same period, 3 out of 16 RUNX1^{mut} mice developed an MDS-like phenotype. Occasionally mice transplanted with miR-146a^{KO} (n = 4/15) BM cells developed a hematologic malignancy during this period. miR-146a^{KO}/RUNX1^{mut} mice had shorter median survival as compared to RUNX1^{mut} mice (319 versus 453 days, p = 0.01). (Figure 1C). At the time of death, miR-146a^{KO}/RUNX1^{mut} mice showed thrombocytopenia, normal levels of white blood cells (WBCs) and reduced red blood cells (RBCs) compared to the other groups, with low hemoglobin and increased mean corpuscular volume (MCV), consistent with macrocytic anemia. (Figures 1D and S1B). While we observed mild signs of ineffective erythropoiesis in the miR-146a^{KO} and RUNX1^{mut} mice, it was more pronounced in the miR-146a^{KO}/RUNX1^{mut} mice (Figure S1C). Primary transplanted miR-146a^{KO}/RUNX1^{mut} mice showed anisocytosis, poikilocytosis, teardrop-shaped RBCs, nucleated RBCs, and variable degrees of polychromasia (Figures 1E and S1C). We also observed several hypersegmented neutrophils in miR-146a^{KO} and miR-146a^{KO}/RUNX1^{mut} mice, but not in control or RUNX1^{mut} mice. Mice engrafted with miR-146a^{KO}/RUNX1^{mut} BM cells developed splenomegaly (Figures 1F, 1G, and S1D), osteopetrosis, and moderate reticulin fibrosis in BM (Figures 1E and S1D). Reticulin fibrosis was also present in BM of miR-146a^{KO} mice, indicating that the loss of miR146a drives this phenotype. At the time of death, miR-146a^{KO}/RUNX1^{mut} mice had increased levels of the macrophage marker F4/80 and the megakaryocyte marker CD61, and reduced levels of thymocytes compared to control mice suggestive of megakaryocytic and monocytic proliferation (Figure S1E). RUNX1^{mut} mice showed elevated Ter119+ cells and lowered CD3+NK1.1 cells in PB compared to control mice (Figure S1E). Based on the Bethesda proposals for the classification of nonlymphoid hematopoietic neoplasms, the miR-146a^{KO}/RUNX1^{mut} mice developed a BMF with myelofibrosis,[28] resembling human MDS with fibrosis.[29]

Persistence of miR-146a^{KO}/RUNX1^{mut} HSPCs results in overt AML

To evaluate disease progression, we next performed secondary and tertiary transplantations into lethally irradiated WT mice using the RUNX1^{mut} or miR-146a^{KO}/RUNX1^{mut} BM cells isolated from the primary recipient mice. The overall survival of mice engrafted with miR-146a^{KO}/RUNX1^{mut} BM cells was shorter than mice engrafted with RUNX1^{mut} cells following the secondary (median survival of 258 days versus 489 days, respectively) and tertiary transplants (median survival of 84 days versus 252 days, respectively) (Figure 2A). In secondary transplants, miR-146a^{KO}/RUNX1^{mut} exhibited anemia and erythroid dysplasia (Figures 2B and 2C). Flow cytometric and histologic examination at the time of death showed an expansion of myeloid blasts in the BM and spleen, and blast infiltration into the liver (Figures 2D, 2E, S2A, and S2B). The number of WBCs was also elevated in miR-146a^{KO}/RUNX1^{mut} mice (Figure S2C), and the percentage of miR-146a^{KO}/RUNX1^{mut} GFP/c-kit double-positive cells in PB was significantly increased as compared to RUNX1^{mut} cells (Figure 2F). The percentage of GFP/c-kit double-positive cells in the BM was comparable between the groups (Figure S2D). To confirm that the myeloid blasts were derived from miR-146a^{KO}/RUNX1^{mut} cells, GFP+ and GFP− BM cells were isolated and examined morphologically. The miR-146a^{KO}/RUNX1^{mut} (GFP+) cells showed evidence of myeloid blasts, while the GFP negative (GFP−) cells were primarily neutrophil bands, mature myeloid cells, and transit-amplifying cells (Figure S2E). To examine erythroid maturation in secondary transplanted miR-146a^{KO}/RUNX1^{mut} mice, we analyzed cell surface markers CD71 and Ter119. At the time of death, we observed the increased proportions of the immature S1 population (CD71^{high}/Ter119$^-$; 30.9%
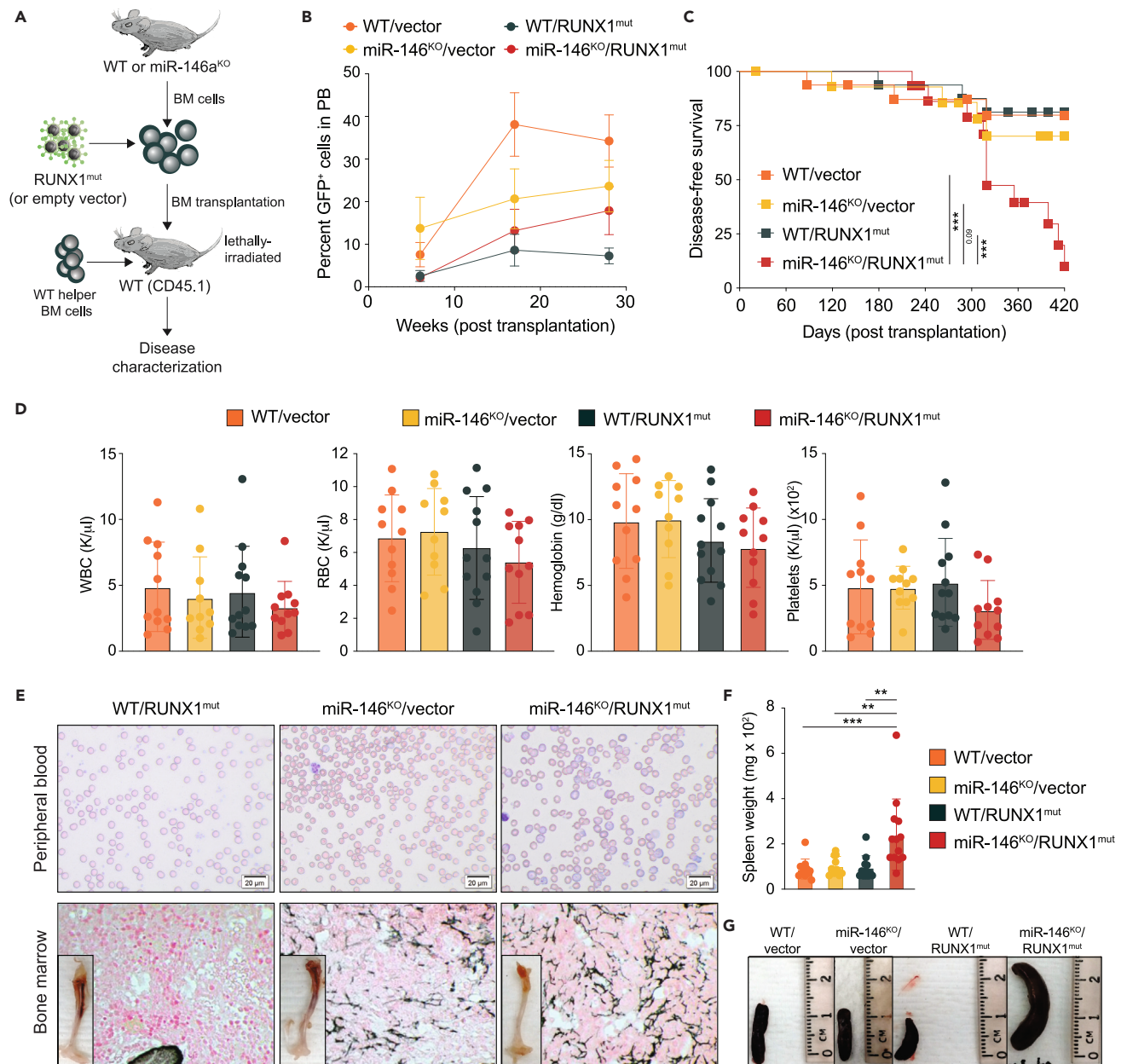
Figure 1. Loss of miR-146a and RUNX1 mutant cooperate to induce an MDS-like disease

(A) Schematic of experimental design for primary BM transplants.

(B) Percentage of GFP-positive cells in PB post-transplantation measured by flow cytometry.

(C) Kaplan-Meier survival curve for primary BM transplanted mice.

(D) PB counts from primary transplanted mice at time of death. WBC, white blood cell; RBC, red blood cell.

(E) Representative images of Giemsa staining of PB smears (upper panel) or reticulin staining of BM (lower panel) from primary transplanted mice at time of death. A representative femur is shown in the lower panel. Magnification 40×.

(F) Spleen weight of primary transplanted mice at time of death.

(G) Representative pictures of the spleen. WT, wild type; KO, knockout; mut, mutant. Error bars represent the standard error of mean. *, $p < 0.05$; **, $p < 0.01$; ***, $p < 0.001$.

versus 10.8% in controls) and reduced proportions of the S4 population (CD71$^+$/Ter119^{high}; 1.8% versus 9.6% in controls), indicating a block in erythroid maturation of miR-146a^{KO}/RUNX1^{mut} cells (Figures S2F and S2G).

When miR-146a^{KO}/RUNX1^{mut} BM cells were transplanted into tertiary recipients, the disease was fatal with a median survival of 8 weeks (Figure 2A). The miR-146a^{KO}/RUNX1^{mut} mice were diagnosed with either AML or MDS with excess blasts (MDS-EB). Although RUNX1^{mut} cells
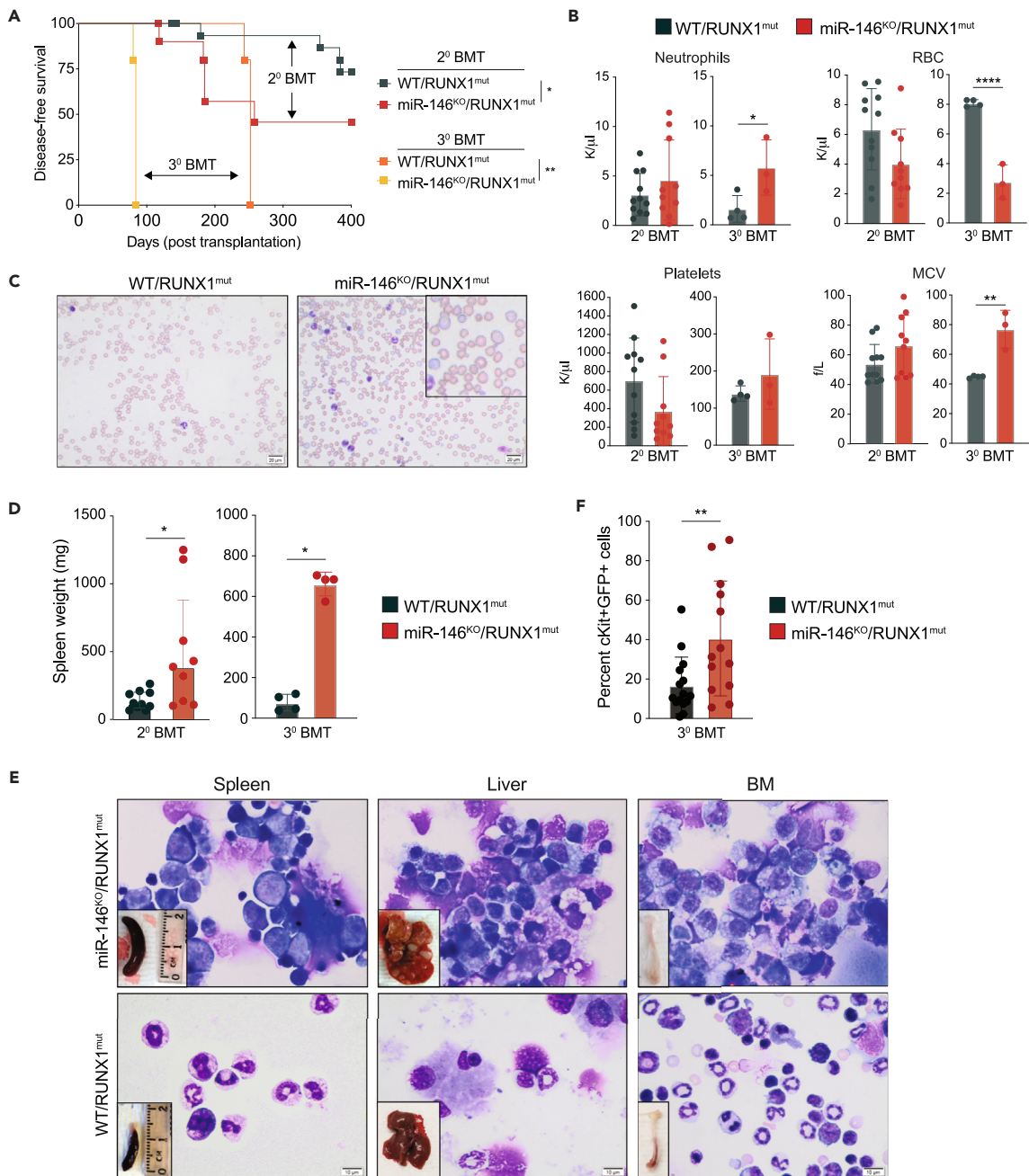
Figure 2. Preleukemic miR-146a^{KO}/RUNX1^{mut} HSPCs progress to overt AML

(A) Kaplan-Meier survival curve for secondary (2^0, $n = 7$/group) and tertiary (3^0, $n = 5$/group) BM transplanted mice (BMT). Arrows indicate the mice group comparisons.

(B) PB counts from serially transplanted mice at the time of death.

(C) Representative Wright-Giemsa staining of PB smears from secondary transplanted mice at the time of death. 40× magnification.

(D) Spleen weights of secondary and tertiary BM transplanted mice.

(E) Representative Wright-Giemsa staining of spleen, BM, and liver cytospins from secondary transplanted mice at the time of death. Magnification 100×. A representative spleen, liver, and femur are shown in the lower left corner.

(F) Percentage of double cKit- and GFP-positive cells in PB post-transplantation measured by flow cytometry. WT, wild type; KO, knockout; mut, mutant. Error bars represent the standard error of mean. *, $p < 0.05$; **, $p < 0.01$; ***, $p < 0.001$; ****, $p < 0.0001$.

repopulated mice following secondary and tertiary transplantations, mice engrafted with RUNX1[mut] cells did not progress to overt myeloid leukemia (Figure 2A). Several mice engrafted with RUNX1[mut] cells became anemic and developed solid tumors (in the liver or abdominal cavity), presenting with enlarged thymus or splenomegaly (data not shown).

RUNX1[mut] is necessary for the expansion of preleukemic miR-146a[KO] HSPCs

To determine the cellular basis for the accelerated disease progression and AML development in mice engrafted with miR-146a[KO]/RUNX1[mut] BM cells, we examined hematopoietic cell populations. We first evaluated the chimerism of CD45.2^{+}GFP^{+} cells in myeloid and lymphoid populations in PB postsecondary transplantation. Transgene-expressing (GFP+) mature lymphoid (CD19^{+} and CD3^{+}) and myeloid (CD11b+) cells were produced, to varying degrees by miR-146a[KO]/vector, WT/RUNX1[mut], and miR-146a[KO]/RUNX1[mut] mice related to control mice at 22 weeks (Figure 3A). Although miR-146a[KO]/vector mice produced myeloid and lymphoid cells, we detected low proportions of long-term hematopoietic stem cells (LT-HSCs), short-term hematopoietic cells (ST-HSCs), and multipotent progenitor cells (MPPs) derived from the miR-146a[KO]/vector (GFP+) cells at time of death (Figure 3B). As expected, the proportions of RUNX1[mut] expressing cells were not significantly different from WT cells (Figure 3B). In contrast, miR-146a[KO]/RUNX1[mut] LT-HSCs, ST-HSCs, and MPPs were significantly expanded as compared to the miR-146a[KO]/vector cohort (Figure 3B). The differences among the HSPC populations were not attributed to differences in BM cellularity (Figure S3A). These findings suggest that expression of RUNX1[mut] restores the attrition of miR-146a[KO] HSPCs, which are primed for leukemic transformation. Moreover, immature cKit+ cells were expanded in the PB of miR-146a[KO]/RUNX1[mut] mice as compared to either miR-146[KO] or RUNX1[mut] cohorts following secondary transplantations (Figure 3C). This expansion was restricted to the miR-146a[KO]/RUNX1[mut] cells as non-transgene expressing cells (GFP−) did not exhibit expansion of cKit+ cells (Figure S3B).

To examine the function of isolated miR-146a[KO]/RUNX1[mut] HSPCs, the progenitor frequency was determined by serial replating in methylcellulose assays of sorted GFP^{+} LSK cells. Consistent with a decline of miR-146a[KO]/vector HSPCs in secondary transplanted mice, miR-146a[KO]/vector LSK cells (GFP+) isolated from primary transplanted mice exhausted after two rounds of replating (Figure 3D). In contrast, miR-146a[KO]/RUNX1[mut] LSKs resulted in serial replating (Figure 3D). These findings suggest that chronic innate immune activation, such as via loss of miR-146a, results in attrition of HSPCs; however, a second hit mutation, such as RUNX1, rescue the fitness advantage of these defective HSPCs in vivo.

To further explore the cellular basis for expansion of miR-146a[KO]/RUNX1[mut] HSPCs, we examined cell proliferation in vivo by administering BrdU into primary recipient mice. We observed increased proportion of BrdU incorporation into miR-146a[KO] and miR-146a[KO]/RUNX1[mut] (GFP[+]) ST-HSCs as compared with control or RUNX1[mut] cells (Figure 3E). There were no observed differences in apoptosis in BM and spleen cells (Figure S3C). These results reveal that the RUNX1[mut] rescues the hematopoietic repopulation deficiency of miR-146a[KO] HSPCs and suggest that RUNX1[mut] is necessary for the clonal expansion of preleukemic miR-146a[KO] HSPCs.

Increased systemic inflammation is widely observed in MDS and AML and is associated with worse outcomes.[30,31] To investigate the inflammatory state of diseased mice engrafted with miR-146a[KO]/RUNX1[mut] cells, we examined cytokines levels in the PB plasma of primary and secondary recipient mice (from Figure 2). The levels of IL6, TNFα, and MCP1 were trending higher in mice engrafted with miR-146a[KO]/RUNX1[mut] cells as compared to miR-146a[KO], RUNX1[mut], or WT mice (Figure S4). Therefore, RUNX1[mut] maintains or can exacerbate the inflammatory phenotype of miR-146a[KO] HSPCs in diseased mice.

Cooperating proto-oncogenes or tumor suppressor genes do not contribute to the transformation of miR-146a[KO]/RUNX1[mut] HSPCs

Previous studies implicated chronic inflammation as a contributing factor to DNA damage leading to the accumulation of mutations and various epigenetic changes in cells.[32,33] To investigate whether deletion of miR-146a results in DNA damage in the leukemic cells, we performed whole exome sequencing of miR-146a[KO]/RUNX1[mut] HSPCs (GFP+) isolated from independent moribund mice (n = 3) along with control mice (WT/vector, WT/RUNX1[mut], and miR-146a[KO]/vector) (Figure 4A). The frequency of single nucleotide polymorphism (SNP) and insertions or deletions (INDEL) was not significantly elevated in leukemic miR-146a[KO]/RUNX1[mut] mice (Figure 4B). RUNX1 mutations can cause AML in murine retroviral transduction and BMT models, typically after retroviral vector insertion mutagenesis at Evi1 or Mn1 loci.[25] Therefore, we next determined whether the prolonged latency of AML in mice engrafted with miR-146a[KO]/RUNX1[mut] cells is due to retroviral integration adjacent to known cooperating genes. Through analysis of the provirus sequences in the exome sequencing analysis, we confirmed proviral integrations from 1 to 10 per mouse (Figure 4C; Table S1). Examination of the proviral integrations also revealed potentially impacted neighboring host genes. In some cases, such as for miR-146a[KO]/RUNX1[mut] mouse #3, no neighboring genes were identified. Importantly, none of the proviral integrations occurred in genes with known roles in leukemia development (Figure 4C; Table S1). Collectively, the AML phenotypes observed in miR-146a[KO]/RUNX1[mut] mice are not due to genomic instability or from opportunistic activation of proto-oncogenes or inactivation of tumor suppressor genes from retroviral integration.

RUNX1[mut] rewires the transcriptome of preleukemic miR-146a[KO] HSPCs

To identify the molecular basis of how miR-146a[KO]/RUNX1[mut] HSPCs gain a fitness advantage and progress to AML, we performed RNA sequencing on LSK (GFP+) isolated from secondary recipient mice engrafted with miR-146a[KO]/RUNX1[mut], miR-146a[KO], RUNX1[mut], or WT HSPCs (Figure 5A). Principal component analysis (PCA) showed that miR-146a[KO] LSK have a gene expression pattern distinct from miR-146a[KO]/RUNX1[mut], RUNX1[mut], or WT LSKs (Figure 5B). Among the groups, miR-146a[KO] LSK had the greatest number of dysregulated genes (n = >800, fold change > |1.5|, p < 0.05) compared to WT controls (Figure 5C). As previously reported, we observed broad dysregulation of
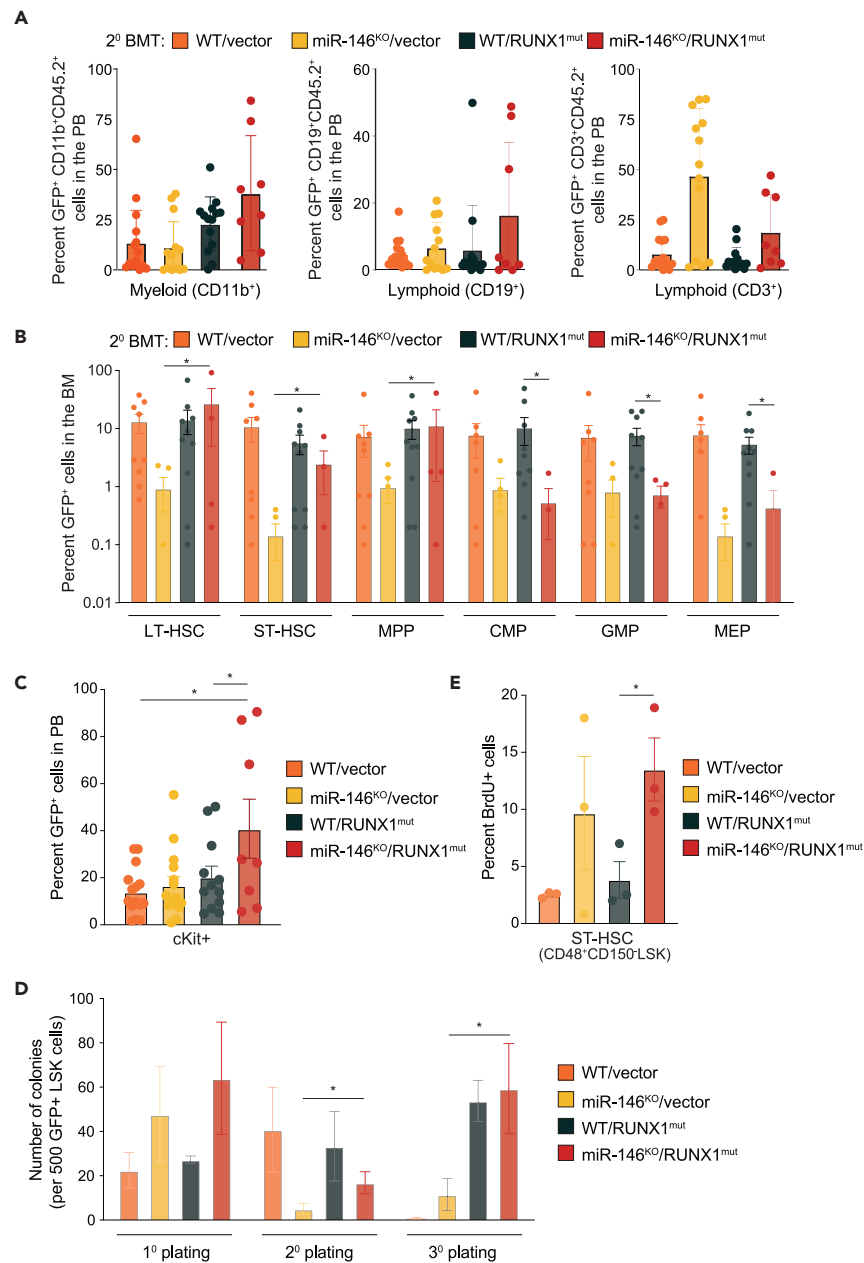
Figure 3. RUNX1[mut] is necessary for the expansion of preleukemic miR-146a[KO] HSPCs

(A) Percentage of GFP+ myeloid and lymphoid cells in PB of secondary transplanted mice at time of death determined by flow cytometry.

(B) Percentage of hematopoietic stem and progenitor cells expressing GFP in BM of secondary transplanted mice. *, $p < 0.01$.

(C) Donor-derived (GFP+) c-Kit+ cells in PB of secondary transplanted mice determined by flow cytometry.

(D) Colony assay of LSK cells from secondary transplanted mice at time of death.

(E) Proliferation of short-term hematopoietic cells (ST-HSC) from transplanted mice measured by bromouridine incorporation. Error bars represent the standard error of mean (A, B, C, and E) and standard deviation (D). *, $p < 0.05$; **, $p < 0.01$; ***, $p < 0.001$; ****, $p < 0.0001$.

innate and adaptive immune signaling in miR-146a[KO] versus WT (empty vector) LSK cells[9,16–18,34] (Figure 5D; Tables S2 and S3). In contrast, RUNX1[mut] LSK cells had the fewest gene expression changes ($n = 129$) as compared to WT LSK (48 upregulated and 81 downregulated, fold change >|1.5|, $p < 0.05$) (Figure 5C; Tables S4 and S5). Interestingly, miR-146a[KO]/RUNX1[mut] LSK cells had fewer dysregulated genes ($n = 176$) as compared to miR-146a[KO] LSK (Figure 5C), suggesting that RUNX1[mut] is altering the transcriptome in miR-146a[KO] HSPCs. Among the down-regulated genes are those involved in interferon (IFN) regulation (*Cd27* and *Il27ra*), cell differentiation (*Prdm16*, *Nkx2-3*, *Dzip1*, and *Bex1*), genes that regulate B and T cell function (*Slamf1*, *Tnfsf4*, *Il27ra*, *Bcl11a*, *Bcl2*, and *Nfat5*), while upregulated genes belonged to the innate
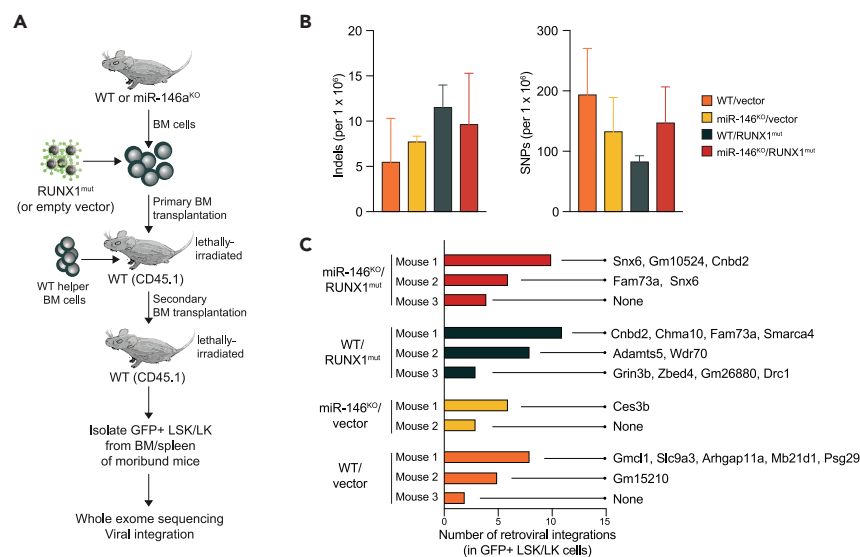
Figure 4. Whole exome sequencing and pro-viral integration analysis of miR-146a^{KO}/RUNX1^{mut} HSPCs

(A) Schematic of experimental design for the exome sequencing analysis of LK and LSK cells from secondary transplanted mice.

(B) Number of insertions-deletions (indels) and single nucleotide polymorphisms (SNPs) determined by whole exome sequencing detected in sorted GFP+ LSK/ LK cells from secondary transplanted mice at time of death.

(C) Number of retroviral integrations detected in GFP+ LSK/LK of secondary transplanted mice. Genes with retroviral integrations are indicated. A comprehensive list of genes is in Table S2. Error bars are the standard deviation.

immune response (*Tlr1*, *Tlr7*, *Tlr13*, *C4b*, *Cfp*, and *ifi204*), inflammation (*Chil3*, *CD163*, *Csf1r*, and *Spic*), cell adhesion (*Cd36*, *Itga9*, *Itgb2*, *Itgb5*, and *Siglec1*), osteoclast differentiation (*Fcgr1*, *Fcgr3*, *Fcgr4*, and *Ncf2*), and master regulators of normal and malignant hematopoiesis (*Msi2*, *Gfi1*, and *Bcl6*) (Figure 5D; Table S4). Although the number of dysregulated genes in miR-146a^{KO}/RUNX1^{mut} LSK was significantly fewer than in miR-146a^{KO} LSK, the miR-146a^{KO}/RUNX1^{mut} LSKs exhibited a greater enrichment of genes related to innate immune responses as compared to miR-146a^{KO} LSK (Figure 5D; Tables S6 and S7). These findings suggest that deletion of miR-146a results in broad gene dysregulation and that a second hit RUNX1 mutation consolidates the transcriptional responses to ones primarily related to immune signaling and malignant hematopoiesis.

To identify the transcriptional changes that might be contributing to the leukemic phenotype in the miR-146a^{KO}/RUNX1^{mut} HSPCs, we intersected the differentially expressed genes (DEGs) among miR-146a^{KO}/RUNX1^{mut}, miR-146a^{KO}, and RUNX1^{mut} LSKs (Figure 5E). miR-146a^{KO}/RUNX1^{mut} HSPCs exhibited 62 unique DEG (Figure 5E). The genes unique to miR-146a^{KO}/RUNX1^{mut} HSPCs are involved in regulation of innate immunity (*FCGR1*, *BCL6*, *CD300A*, *PRKCE*, *GPR183*, and *SLAMF1*), malignant hematopoiesis (*MSI2*, *GFI1*, *BCL6*, *PRDM16*, *BCL11A*, and *BCL2*), and cell adhesion (*PRKCE*, *CLDN13*, *NCAM1*, *MUC4*, *SIGLECF*, and *SLAMF1*)[35–42] (Figures 5F and 5G; Table S8).

To determine whether RUNX1 directly regulates the expression of the genes unique to miR-146a^{KO}/RUNX1^{mut} HSCPs, we evaluated RUNX1 genome wide occupancy in murine and human hematopoietic cells. We first compiled all RUNX1 chromatin immunoprecipitation sequencing (ChIP-seq) analyses (21 mouse and 31 human ChIP-seq GEO datasets) performed in healthy and leukemic hematopoietic cells and then identified genomic locations bound by RUNX1 (Table S9). To determine whether these RUNX1 bound regions are associated with the transcriptional changes in miR-146a^{KO}/RUNX1^{mut} LSK, we assigned RUNX1 ChIP peaks to the 62 unique DEGs miR-146a^{KO}/RUNX1^{mut} LSKs by proximity within the context of the topologically associated domain. RUNX1 bound regions were nominated if they were present in >50% of the datasets. Twenty-three and 7 of the DEGs were identified exclusively in human or mouse ChiP-seq datasets so these were excluded from further analysis (Figure 5H). We observed human and mouse RUNX1 peaks adjacent to 35 of the 62 DEGs (Figure 5H; Table S10). The RUNX1 bound genes that are differentially expressed in miR-146a^{KO}/RUNX1^{mut} LSKs include regulators of HSC expansion (i.e., *BCL2*, *MSI2*, and *GFI1*) and differentiation (i.e., *PRDM16*, *TIFAB*, and *CDH3*), innate and adaptive immune signaling (i.e., *SLAMF1*, *CD27*, *GPR183*, *IL27RA*, and *NFAT5*), and cytokine production (i.e., *SYT11*, *SLAMF1*, and *IL27RA*) (Figure 5I). These observations suggest that RUNX1^{mut} rewires the transcriptome of preleukemic miR-146a^{KO} HSPCs resulting in sustained expression of innate immune and stem cell genes.

Given that dysregulated innate immune and inflammatory signaling pathways are sustained by miR-146a^{KO}/RUNX1^{mut} AML cells, we wanted to investigate whether these pathways remain critical for the leukemic cells. We evaluated an inhibitor (NSC697923) that targets TRAF6, a key target of miR-146a in MDS/AML, via inhibition of its co-factor UBE2N.[43,44] Treatment with NSC697923 abolished colony formation by miR-146a^{KO}/RUNX1^{mut} AML cells while not impacting WT/vector hematopoietic cells (Figures 5J and S5). These findings suggest that cell-intrinsic innate immune signaling is not only required for initiating AML but is also required for sustaining the leukemic phenotype. Collectively, we provide evidence that dysregulation of innate immune and inflammatory signaling contributes to the progression and maintenance of AML.
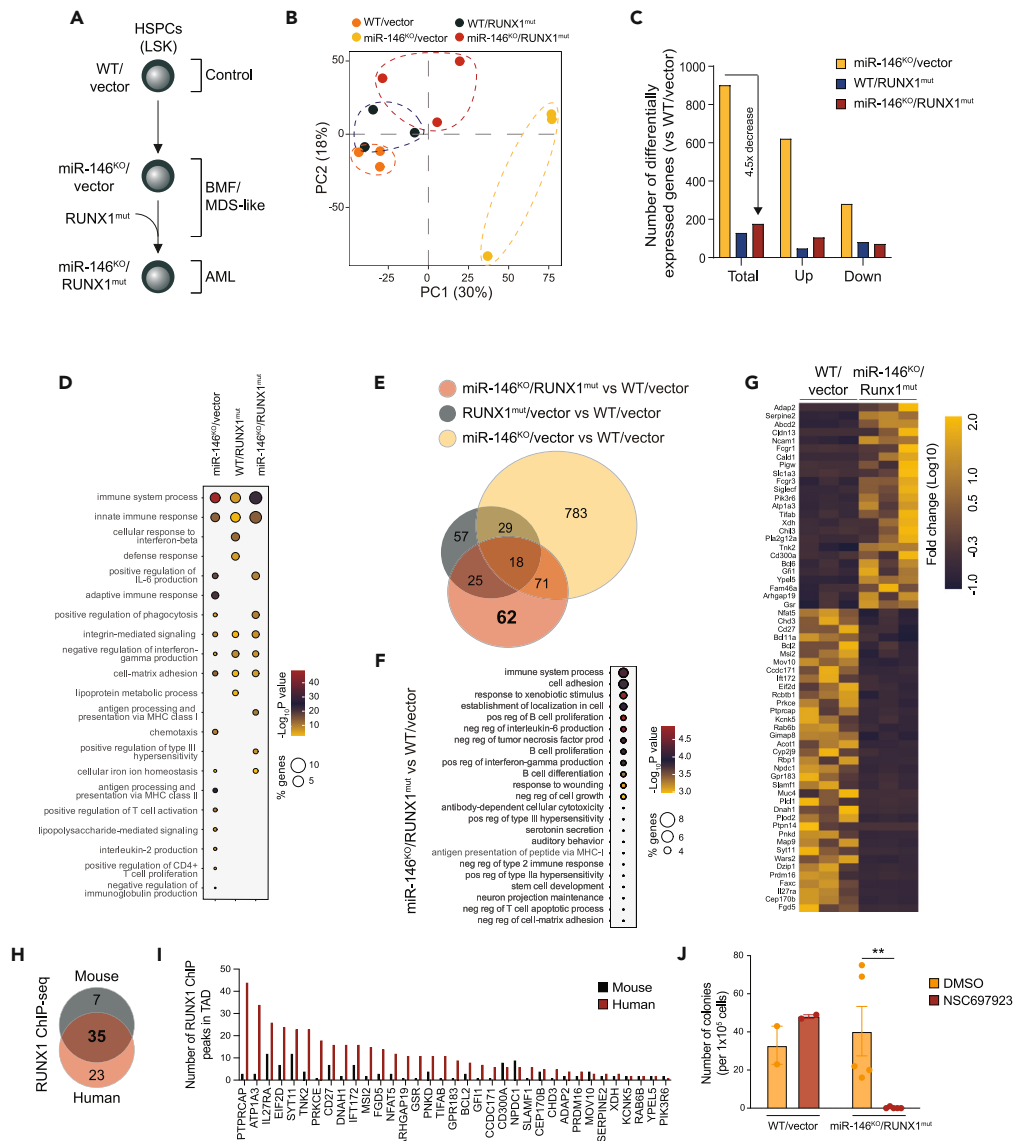
Figure 5. RUNX1^{mut} rewires the transcriptome of preleukemic miR-146a^{KO} HSPCs

(A) Schematic of experimental design for the RNA sequencing (RNA-seq) analysis of GFP+ LSK cells from secondary transplanted mice. Phenotypes of each of the mouse models are indicated.

(B) Principal component analysis of RNA-seq samples for each of the mouse model groups. Each dot represents a sample. A dotted line was manually added to aid in the visualization of sample grouping.

(C) Bar graph indicating the number of differentially expressed genes (DEGs) in each of the mouse models compared to wild-type/vector mice. Total DEGs, unregulated (up), and downregulated (down) genes are indicated.

(D) Balloon plot showing the gene set enrichment analysis for the DEGs including GO terms biological processes. The size of the circles corresponds with the percent of enriched genes in each category. The color indicates the statistical significance, with red mapping to the most significant value.

(E) Venn diagram intersecting the DEGs in LSK cells in each of the mouse models. DEGs unique to miR-146a^{KO}/RUNX1^{mut} LSK cells are indicated in bold.

(F) Balloon plot for gene set enrichment for the DEGs in miR-146a^{KO}/RUNX1^{mut} LSK cells. The size of the circles corresponds with the percent of enriched genes in each category. The color indicates the statistical significance, with red mapping to the most significant value.

(G) Heatmap of the 62 DEGs unique to miR-146a^{KO}/RUNX1^{mut} LSK cells. Upregulated genes appear in yellow and downregulated genes appear in blue. The scale on the right represents the row Z score.

(H) Venn diagram intersecting the genes with RUNX1 ChIP peaks in mouse and human hematopoietic cells. Only the DEGs in miR-146a^{KO}/RUNX1^{mut} LSK cells are considered in this analysis.

(I) Bar graph showing the number of RUNX1 ChIP-seq peaks found near the DEGs in miR-146a^{KO}/RUNX1^{mut} LSK cells in mouse and human public samples.

(J) Colony formation assay of WT/vector and miR-146a^{KO}/RUNX1^{mut} GFP+LSK cells treated with NSC697923 (2 µM). Error bars are the standard error of mean. *, $p < 0.05$; **, $p < 0.01$; ***, $p < 0.001$; ****, $p < 0.0001$.

DISCUSSION

Cell-intrinsic dysregulation of innate immune and inflammatory-related pathways as well as systemic inflammation are implicated in hematopoietic defects associated with myeloid malignancies. Various genetic and molecular changes affect innate immune- and inflammatory-related pathways. There is also substantive evidence of microenvironment changes within the MDS and AML BM niche. More recent findings have supported the premise that dysregulated innate immune and inflammatory pathways in leukemic cells do not result in increased pathway activation, but rather alter their response to the microenvironment in a way that favors the competitive advantage of leukemic clones.[3] Muto et al. found that preleukemic HSPCs are protected from chronic inflammation compared to normal HSPCs.[45] In response to inflammation, preleukemic HSPCs switch from canonical to noncanonical NF-κB signaling, which is dependent on TLR-TRAF6-mediated activation of A20.[45] ASXL1 mutations also promote clonal dominance by altering their response to inflammation by expressing negative regulators of inflammatory signaling.[46] TET2-deficient myeloid cells and HSPCs acquire resistance to IL6-mediated inflammatory stress by increasing expression of the anti-apoptotic lncRNA Morrbid.[47] In separate studies, TET2-deficient HSPCs that have impaired TLR-TRAF6 signaling can malignantly transform to AML.[44] IFNγ signaling during chronic infection can drive DNMT3A-loss-of-function clonal hematopoiesis and mimic clonal hematopoiesis by becoming unresponsive to IFNy-induced stress.[48] Collectively, these studies reveal how preleukemic and leukemic clones disrupt the stoichiometry of key innate-immune relating signaling hubs in a way that alters their circuitry and adaptations that allow for their outgrowth.

In certain cases, response to inflammatory stress can result in maladaptive changes to leukemic HSPCs. In a model of del(5q)-like MDS, inflammation impaired del(5q)-like HSPCs, leading to reduced numbers, premature attrition, and increased p53 expression.[49] The functional defect of the del(5q)-like MDS was restored by p53 deletion. The findings suggest that inflammation provides a competitive advantage to functionally defective del(5q) HSPCs upon p53 loss, potentially influencing the selective pressure for genetic inactivation of p53 or expansion of a pre-existing TP53-mutant clone in del(5q) AML following an MDS diagnosis. Herein, we propose a distinct mechanism by which a second hit mutation directly alters cell-intrinsic innate immune signaling, a step necessary for malignant transformation. Expression of RUNX1^{mut} rescued the hematopoietic repopulation deficiency of miR-146a^{KO} HSPCs. Although deletion of miR-146a results in broad dysregulation of innate immune and inflammatory pathways, expression of RUNX1^{mut} in miR-146a^{KO} HSPCs restricted the expression of these pathways to a subset of innate immune and inflammatory genes at the AML stage. These findings represent evidence that dysregulation of innate immune and inflammatory signaling is required for propagating preleukemic cells and contributes to the progression of AML. While we describe cooperation between RUNX1 mutations and the dysregulation of cell-intrinsic innate immune signaling (resulting from the loss of miR-146a), the exact mechanistic basis remains unknown and necessitates further investigation.

RUNX1 or *AML1* encodes a transcription factor with location on chromosome 21q22 and is the most frequent target for chromosomal translocation in leukemia.[50,51] RUNX1 mutations can cause MDS/AML in murine retroviral transduction mediated overexpression and BMT models; however, the latency is long and retroviral vector insertion mutagenesis at *Evi1* or *Mn1* loci seems critical for MDS/AML development in these models.[25] Germline mutations in the RUNX1 gene, typically at R188Q, are also implicated in causing familial platelet disorder (FPD), which have an associated risk of MDS/AML.[20] Runx1^{R188Q} HSPCs exhibited defective DNA-damage response, reduced differentiation of long-term repopulating HSCs, and enhanced competitive capacity, but do not develop MDS/AML.[52] Thus, RUNX1 mutations require a cooperating mutation to induce overt disease. Furthermore, RUNX1 mutations are linked to altered innate immune and inflammatory signaling. RUNX1 is crucial for epigenetically repressing two inflammatory signaling pathways: TLR4 and type I IFN signaling.[23,24] Loss of RUNX1 in granulocyte-monocyte progenitors (GMPs) increases neutrophils' inflammatory response to lipopolysaccharides (LPS), partly through elevated CD14 expression.[24] RUNX1 binds CD14 and other genes in the TLR4 and IFN pathways, leading to increased chromatin accessibility when RUNX1 is absent. Consistent with these observations, Runx1^{R188Q} mutation in mice lead to increased HSPCs, in part due to systemic inflammation.[52] In human HSPCs, RUNX1 loss also reduces proliferative capacity and stem cell function by selectively upregulating the IL-3 receptor.[53] Exposure to IL-3 rescues proliferative and competitive defects in RUNX1-deficient cells. These studies highlight the complex interplay between RUNX1 function and inflammatory signaling in hematopoietic cells and support our findings that chronic activation of innate immune signaling cooperates with mutant RUNX1 to drive the progression from preleukemia to AML.

There has been growing interest in targeting innate immune pathways in preleukemic and leukemic conditions.[54–57] We showed that inhibition of innate immune signaling with an UBE2N inhibitor was sufficient to suppress the leukemic miR-146a^{KO}/RUNX1^{mut} HSPCs. These findings suggest that dysregulated innate immune and inflammatory signaling contribute to the pathogenesis of myeloid malignancies but also that these pathways remain necessary for maintaining the leukemic cells. Additional genetic studies are needed to precisely define which innate immune and inflammatory effectors are critical for sustaining the leukemic phenotypes in the miR-146a^{KO}/RUNX1^{mut} model. In prior studies, we found that UBE2N is required for leukemic cell function *in vitro* and *in vivo* by maintaining oncogenic immune signaling states.[58] UBE2N (Ubc13) is a ubiquitin-conjugating enzyme implicated in the regulation of TRAF6, an E3 ubiquitin ligase and effector of the TLR/IL1R signaling pathway.[59] Using small-molecule inhibitors identified in *in silico* structure-based and cellular-based screens, we revealed the therapeutic efficacy of interfering with UBE2N function by blocking of ubiquitination of innate immune- and inflammatory-related substrates in human AML cells.[58] Inhibition of UBE2N function disrupted oncogenic immune signaling by promoting cell death of leukemic HSPCs while sparing normal HSPCs *in vitro*.[58] In a clonal evolution model of AML using induced pluripotent stem cells (iPSC), Wang et al. found that the earliest persistent signaling alterations involve genes related to inflammation and innate immunity.[60] Targeting inflammatory signaling with UBE2N or IRAK1/4 inhibitors in the iPSC progression model exerted inhibitory effects at all disease stages, suggesting that modulation of inflammatory signaling as a therapeutic avenue for early-stage intervention in MDS and AML.[60] Importantly, our data herein provide further evidence of the importance of dysregulated innate immune and inflammatory signaling for propagating preleukemic cells and its contribution to the progression and maintenance of AML.

Limitations of the study

The study has several limitations that warrant consideration. Firstly, the use of a retroviral approach to express RUNX1^{mut} may introduce variability and non-physiological gene expression, potentially affecting the development of the observed phenotypes. Additionally, serial BM transplantations induce additional layers of hematopoietic stress, which may influence disease development. Furthermore, while miR-146a is a key gene within the del(5q) segment in MDS and AML, we acknowledge that other genes within the deleted region may also play a role in disease progression in cooperation with RUNX1^{mut}. Moreover, while our *in vitro* studies demonstrate the importance of TRAF6-UBE2N signaling in AML cell function, future research should explore the development of AML *in vivo* to fully understand its implications. Lastly, the exact cellular and molecular mechanisms underlying the cooperation between RUNX1 mutations and dysregulation of cell-intrinsic innate immune signaling via miR-146a loss remain unclear, suggesting the need for further investigation.

STAR★METHODS

Detailed methods are provided in the online version of this paper and include the following:

- KEY RESOURCES TABLE
- RESOURCE AVAILABILITY
  - Lead contact
  - Materials availability
  - Data and code availability
- METHOD DETAILS
  - Mouse models
  - Retroviral vectors, packaging cell lines, and bone marrow transplantation
  - Cell cycle analysis
  - Colony forming assay
  - Hematological analysis
  - Flow cytometry
  - RNA sequencing
  - Quantitative PCR
  - Cytokine analysis
  - Hematoxylin and eosin staining of BM
  - Peripheral blood, spleen and bone marrow histology
  - Whole exome sequencing
  - ChiP-sequencing analysis
- QUANTIFICATION AND STATISTICAL ANALYSIS

SUPPLEMENTAL INFORMATION

Supplemental information can be found online at https://doi.org/10.1016/j.isci.2024.109809.

AUTHOR CONTRIBUTIONS

L.B. and A.M.S. performed experiments, analyzed and interpreted data, and wrote the manuscript. K.H., S.C., V.R., M.W., and K.G. performed experiments and analyzed and interpreted data. K.C. and M.P. performed bioinformatics analyses. D.W. evaluated the pathology of the models. G.H. provided input and reagents and interpreted data. D.T.S. conceived and directed the study, analyzed and interpreted data, and wrote and/or edited the manuscript. All authors approved the final version of the manuscript.

DECLARATION OF INTERESTS

D.T.S. serves on the scientific advisory board at Kurome Therapeutics and is a consultant for and/or received funding from Kurome Therapeutics, Captor Therapeutics, Treeline Biosciences, and Tolero Therapeutics. D.T.S. has equity in Kurome Therapeutics. L.B. is a current employee of Johnson and Johnson Innovative Medicine and an equity holder in a publicly traded company.

REFERENCES

1. Menssen, A.J., and Walter, M.J. (2020). Genetics of progression from MDS to secondary leukemia. Blood *136*, 50–60. https://doi.org/10.1182/blood.2019000942.

2. Bănescu, C., Tripon, F., and Muntean, C. (2023). The Genetic Landscape of Myelodysplastic Neoplasm Progression to Acute Myeloid Leukemia. Int. J. Mol. Sci. *24*, 5734. https://doi.org/10.3390/ijms24065734.

3. Trowbridge, J.J., and Starczynowski, D.T. (2021). Innate immune pathways and inflammation in hematopoietic aging, clonal hematopoiesis, and MDS. J. Exp. Med. *218*, e20201544. https://doi.org/10.1084/jem.20201544.

4. Barreyro, L., Chlon, T.M., and Starczynowski, D.T. (2018). Chronic immune response dysregulation in MDS pathogenesis. Blood *132*, 1553–1560. https://doi.org/10.1182/blood-2018-03-784116.

5. Sallman, D.A., and List, A. (2019). The central role of inflammatory signaling in the pathogenesis of myelodysplastic syndromes. Blood *133*, 1039–1048. https://doi.org/10.1182/blood-2018-10-844654.

6. Varney, M.E., Melgar, K., Niederkorn, M., Smith, M., Barreyro, L., and Starczynowski, D.T. (2015). Deconstructing innate immune signaling in myelodysplastic syndromes. Exp. Hematol. *43*, 587–598. https://doi.org/10.1016/j.exphem.2015.05.016.

7. Stickel, N., Prinz, G., Pfeifer, D., Hasselblatt, P., Schmitt-Graeff, A., Follo, M., Thimme, R., Finke, J., Duyster, J., Salzer, U., and Zeiser, R. (2014). MiR-146a regulates the TRAF6/TNF-axis in donor T cells during GVHD. Blood *124*, 2586–2595. https://doi.org/10.1182/blood-2014-04-569046.

8. Taganov, K.D., Boldin, M.P., Chang, K.J., and Baltimore, D. (2006). NF-kappaB-dependent induction of microRNA miR-146, an inhibitor targeted to signaling proteins of innate immune responses. Proc. Natl. Acad. Sci. USA *103*, 12481–12486. https://doi.org/10.1073/pnas.0605298103.

9. Boldin, M.P., Taganov, K.D., Rao, D.S., Yang, L., Zhao, J.L., Kalwani, M., Garcia-Flores, Y., Luong, M., Devrekanli, A., Xu, J., et al. (2011). miR-146a is a significant brake on autoimmunity, myeloproliferation, and cancer in mice. J. Exp. Med. *208*, 1189–1201. https://doi.org/10.1084/jem.20101823.

10. Pauley, K.M., Satoh, M., Chan, A.L., Bubb, M.R., Reeves, W.H., and Chan, E.K. (2008). Upregulated miR-146a expression in peripheral blood mononuclear cells from rheumatoid arthritis patients. Arthritis Res. Ther. *10*, R101. https://doi.org/10.1186/ar2493.

11. Tang, Y., Luo, X., Cui, H., Ni, X., Yuan, M., Guo, Y., Huang, X., Zhou, H., de Vries, N., Tak, P.P., et al. (2009). MicroRNA-146A contributes to abnormal activation of the type I interferon pathway in human lupus by targeting the key signaling proteins. Arthritis Rheum. *60*, 1065–1075. https://doi.org/10.1002/art.24436.

12. Nahid, M.A., Pauley, K.M., Satoh, M., and Chan, E.K.L. (2009). miR-146a is critical for endotoxin-induced tolerance: IMPLICATION IN INNATE IMMUNITY. J. Biol. Chem. *284*, 34590–34599. https://doi.org/10.1074/jbc.M109.056317.

13. Perry, M.M., Moschos, S.A., Williams, A.E., Shepherd, N.J., Larner-Svensson, H.M., and Lindsay, M.A. (2008). Rapid changes in microRNA-146a expression negatively regulate the IL-1beta-induced inflammatory response in human lung alveolar epithelial cells. J. Immunol. *180*, 5689–5698. https://doi.org/10.4049/jimmunol.180.8.5689.

14. Starczynowski, D.T., Kuchenbauer, F., Argiropoulos, B., Sung, S., Morin, R., Muranyi, A., Hirst, M., Hogge, D., Marra, M., Wells, R.A., et al. (2010). Identification of miR-145 and miR-146a as mediators of the 5q-syndrome phenotype. Nat. Med. *16*, 49–58. https://doi.org/10.1038/nm.2054.

15. Rhyasen, G.W., Bolanos, L., Fang, J., Jerez, A., Wunderlich, M., Rigolino, C., Mathews, L., Ferrer, M., Southall, N., Guha, R., et al. (2013). Targeting IRAK1 as a therapeutic approach for myelodysplastic syndrome. Cancer Cell *24*, 90–104. https://doi.org/10.1016/j.ccr.2013.05.006.

16. Fang, J., Barker, B., Bolanos, L., Liu, X., Jerez, A., Makishima, H., Christie, S., Chen, X., Rao, D.S., Grimes, H.L., et al. (2014). Myeloid malignancies with chromosome 5q deletions acquire a dependency on an intrachromosomal NF-kappaB gene network. Cell Rep. *8*, 1328–1338. https://doi.org/10.1016/j.celrep.2014.07.062.

17. Grants, J.M., Wegrzyn, J., Hui, T., O'Neill, K., Shadbolt, M., Knapp, D.J.H.F., Parker, J., Deng, Y., Gopal, A., Docking, T.R., et al. (2020). Altered microRNA expression links IL6 and TNF-induced inflammaging with myeloid malignancy in humans and mice. Blood *135*, 2235–2251. https://doi.org/10.1182/blood.2019003105.

18. Zhao, J.L., Rao, D.S., Boldin, M.P., Taganov, K.D., O'Connell, R.M., and Baltimore, D. (2011). NF-kappaB dysregulation in microRNA-146a-deficient mice drive the development of myeloid malignancies. Proc. Natl. Acad. Sci. USA *108*, 9184–9189. https://doi.org/10.1073/pnas.1105398108.

19. Varney, M.E., Choi, K., Bolanos, L., Christie, S., Fang, J., Grimes, H.L., Maciejewski, J.P., Inoue, J.I., and Starczynowski, D.T. (2017). Epistasis between TIFAB and miR-146a: neighboring genes in del(5q) myelodysplastic syndrome. Leukemia *31*, 491–495. https://doi.org/10.1038/leu.2016.276.

20. Bellissimo, D.C., and Speck, N.A. (2017). RUNX1 Mutations in Inherited and Sporadic Leukemia. Front. Cell Dev. Biol. *5*, 111. https://doi.org/10.3389/fcell.2017.00111.

21. Sood, R., Kamikubo, Y., and Liu, P. (2017). Role of RUNX1 in hematological malignancies. Blood *129*, 2070–2082. https://doi.org/10.1182/blood-2016-10-687830.

22. Olofsen, P.A., and Touw, I.P. (2020). RUNX1 Mutations in the Leukemic Progression of Severe Congenital Neutropenia. Mol. Cell. *43*, 139–144. https://doi.org/10.14348/molcells.2020.0010.

23. Bellissimo, D.C., Chen, C.H., Zhu, Q., Bagga, S., Lee, C.T., He, B., Wertheim, G.B., Jordan, M., Tan, K., Worthen, G.S., et al. (2020). Runx1 negatively regulates inflammatory cytokine production by neutrophils in response to Toll-like receptor signaling. Blood Adv. *4*, 1145–1158. https://doi.org/10.1182/bloodadvances.2019000785.

24. Zezulin, A.U., Yen, D., Ye, D., Howell, E.D., Bresciani, E., Diemer, J., Ren, J.G., Ahmad, M.H., Castilla, L.H., Touw, I.P., et al. (2023). RUNX1 is required in granulocyte-monocyte progenitors to attenuate inflammatory cytokine production by neutrophils. Genes Dev. *37*, 605–620. https://doi.org/10.1101/gad.350418.123.

25. Watanabe-Okochi, N., Kitaura, J., Ono, R., Harada, H., Harada, Y., Komeno, Y., Nakajima, H., Nosaka, T., Inaba, T., and Kitamura, T. (2008). AML1 mutations induced MDS and MDS/AML in a mouse BMT model. Blood *111*, 4297–4308. https://doi.org/10.1182/blood-2007-01-068345.

26. Harada, H., Harada, Y., Tanaka, H., Kimura, A., and Inaba, T. (2003). Implications of somatic mutations in the AML1 gene in radiation-associated and therapy-related myelodysplastic syndrome/acute myeloid leukemia. Blood *101*, 673–680. https://doi.org/10.1182/blood-2002-04-1010.

27. Harada, H., Harada, Y., and Kimura, A. (2006). Implications of somatic mutations in the AML1/RUNX1 gene in myelodysplastic syndrome (MDS): future molecular therapeutic directions for MDS. Curr. Cancer Drug Targets *6*, 553–565. https://doi.org/10.2174/156800906778194595.

28. Kogan, S.C., Ward, J.M., Anver, M.R., Berman, J.J., Brayton, C., Cardiff, R.D., Carter, J.S., de Coronado, S., Downing, J.R., Fredrickson, T.N., et al. (2002). Bethesda proposals for classification of nonlymphoid hematopoietic neoplasms in mice. Blood *100*, 238–245. https://doi.org/10.1182/blood.v100.1.238.

29. Jain, A.G., Zhang, L., Bennett, J.M., and Komrokji, R. (2022). Myelodysplastic Syndromes with Bone Marrow Fibrosis: An Update. Ann. Lab. Med. *42*, 299–305. https://doi.org/10.3343/alm.2022.42.3.299.

30. Liang, Q., Zhao, J., Zhang, L., Gao, Z., Pan, H., Fang, L., and Shi, J. (2022). Association of systemic inflammatory and autoimmune manifestations with myelodysplastic syndromes: A systematic review and meta-analysis. Medicine (Baltim.) *101*, e31427. https://doi.org/10.1097/MD.0000000000031427.

31. Camacho, V., Kuznetsova, V., and Welner, R.S. (2021). Inflammatory Cytokines Shape an Altered Immune Response During Myeloid Malignancies. Front. Immunol. *12*, 772408. https://doi.org/10.3389/fimmu.2021.772408.

32. Canli, Ö., Nicolas, A.M., Gupta, J., Finkelmeier, F., Goncharova, O., Pesic, M., Neumann, T., Horst, D., Löwer, M., Sahin, U., and Greten, F.R. (2017). Myeloid Cell-Derived Reactive Oxygen Species Induce Epithelial

Mutagenesis. Cancer Cell *32*, 869–883.e5. https://doi.org/10.1016/j.ccell.2017.11.004.

33. Greten, F.R., and Grivennikov, S.I. (2019). Inflammation and Cancer: Triggers, Mechanisms, and Consequences. Immunity *51*, 27–41. https://doi.org/10.1016/j.immuni.2019.06.025.

34. Zhao, J.L., Rao, D.S., O'Connell, R.M., Garcia-Flores, Y., and Baltimore, D. (2013). MicroRNA-146a acts as a guardian of the quality and longevity of hematopoietic stem cells in mice. Elife *2*, e00537. https://doi.org/10.7554/eLife.00537.

35. Kharas, M.G., Lengner, C.J., Al-Shahrour, F., Bullinger, L., Ball, B., Zaidi, S., Morgan, K., Tam, W., Paktinat, M., Okabe, R., et al. (2010). Musashi-2 regulates normal hematopoiesis and promotes aggressive myeloid leukemia. Nat. Med. *16*, 903–908. https://doi.org/10.1038/nm.2187.

36. Park, S.M., Gönen, M., Vu, L., Minuesa, G., Tivnan, P., Barlowe, T.S., Taggart, J., Lu, Y., Deering, R.P., Hacohen, N., et al. (2015). Musashi2 sustains the mixed-lineage leukemia-driven stem cell regulatory program. J. Clin. Invest. *125*, 1286–1298. https://doi.org/10.1172/JCI78440.

37. Marneth, A.E., Botezatu, L., Hönes, J.M., Israël, J.C.L., Schütte, J., Vassen, L., Lams, R.F., Bergevoet, S.M., Groothuis, S., Mandoli, A., et al. (2018). GFI1 is required for RUNX1/ETO positive acute myeloid leukemia. Haematologica *103*, e395–e399. https://doi.org/10.3324/haematol.2017.180844.

38. Kawabata, K.C., Zong, H., Meydan, C., Wyman, S., Wouters, B.J., Sugita, M., Goswami, S., Albert, M., Yip, W., Roboz, G.J., et al. (2021). BCL6 maintains survival and self-renewal of primary human acute myeloid leukemia cells. Blood *137*, 812–825. https://doi.org/10.1182/blood.2019001745.

39. Hu, T., Morita, K., Hill, M.C., Jiang, Y., Kitano, A., Saito, Y., Wang, F., Mao, X., Hoegenauer, K.A., Morishita, K., et al. (2019). PRDM16s transforms megakaryocyte-erythroid progenitors into myeloid leukemia-initiating cells. Blood *134*, 614–625. https://doi.org/10.1182/blood.2018888255.

40. Corrigan, D.J., Luchsinger, L.L., Justino de Almeida, M., Williams, L.J., Strikoudis, A., and Snoeck, H.W. (2018). PRDM16 isoforms differentially regulate normal and leukemic hematopoiesis and inflammatory gene signature. J. Clin. Invest. *128*, 3250–3264. https://doi.org/10.1172/JCI99862.

41. Sunami, Y., Yokoyama, T., Yoshino, S., Takahara, T., Yamazaki, Y., Harada, H., and Nakamura, T. (2022). BCL11A promotes myeloid leukemogenesis by repressing PU.1 target genes. Blood Adv. *6*, 1827–1843. https://doi.org/10.1182/bloodadvances.2021004558.

42. Marcucci, G., Byrd, J.C., Dai, G., Klisovic, M.I., Kourlas, P.J., Young, D.C., Cataland, S.R., Fisher, D.B., Lucas, D., Chan, K.K., et al. (2003). Phase 1 and pharmacodynamic studies of G3139, a Bcl-2 antisense oligonucleotide, in combination with chemotherapy in refractory or relapsed acute leukemia. Blood *101*, 425–432. https://doi.org/10.1182/blood-2002-06-1899.

43. Pulvino, M., Liang, Y., Oleksyn, D., DeRan, M., Van Pelt, E., Shapiro, J., Sanz, I., Chen, L., and Zhao, J. (2012). Inhibition of proliferation and survival of diffuse large B-cell lymphoma cells by a small-molecule inhibitor of the ubiquitin-conjugating enzyme Ubc13-Uev1A. Blood *120*, 1668–1677. https://doi.org/10.1182/blood-2012-02-406074.

44. Muto, T., Guillamot, M., Yeung, J., Fang, J., Bennett, J., Nadorp, B., Lasry, A., Redondo, L.Z., Choi, K., Gong, Y., et al. (2022). TRAF6 functions as a tumor suppressor in myeloid malignancies by directly targeting MYC oncogenic activity. Cell Stem Cell *29*, 298–314.e9. https://doi.org/10.1016/j.stem.2021.12.007.

45. Muto, T., Walker, C.S., Choi, K., Hueneman, K., Smith, M.A., Gul, Z., Garcia-Manero, G., Ma, A., Zheng, Y., and Starczynowski, D.T. (2020). Adaptive response to inflammation contributes to sustained myelopoiesis and confers a competitive advantage in myelodysplastic syndrome HSCs. Nat. Immunol. *21*, 535–545. https://doi.org/10.1038/s41590-020-0663-z.

46. Avagyan, S., Henninger, J.E., Mannherz, W.P., Mistry, M., Yoon, J., Yang, S., Weber, M.C., Moore, J.L., and Zon, L.I. (2021). Resistance to inflammation underlies enhanced fitness in clonal hematopoiesis. Science *374*, 768–772. https://doi.org/10.1126/science.aba9304.

47. Cai, Z., Kotzin, J.J., Ramdas, B., Chen, S., Nelanuthala, S., Palam, L.R., Pandey, R., Mali, R.S., Liu, Y., Kelley, M.R., et al. (2018). Inhibition of Inflammatory Signaling in Tet2 Mutant Preleukemic Cells Mitigates Stress-Induced Abnormalities and Clonal Hematopoiesis. Cell Stem Cell *23*, 833–849.e5. https://doi.org/10.1016/j.stem.2018.10.013.

48. Hormaechea-Agulla, D., Matatall, K.A., Le, D.T., Kain, B., Long, X., Kus, P., Jaksik, R., Challen, G.A., Kimmel, M., and King, K.Y. (2021). Chronic infection drives Dnmt3a-loss-of-function clonal hematopoiesis via IFNgamma signaling. Cell Stem Cell *28*, 1428–1442.e6. https://doi.org/10.1016/j.stem.2021.03.002.

49. Muto, T., Walker, C.S., Agarwal, P., Vick, E., Sampson, A., Choi, K., Niederkorn, M., Ishikawa, C., Hueneman, K., Varney, M., and Starczynowski, D.T. (2023). Inactivation of p53 provides a competitive advantage to del(5q) myelodysplastic syndrome hematopoietic stem cells during inflammation. Haematologica *108*, 2715–2729. https://doi.org/10.3324/haematol.2022.282349.

50. Lam, K., and Zhang, D.E. (2012). RUNX1 and RUNX1-ETO: roles in hematopoiesis and leukemogenesis. Front. Biosci. *17*, 1120–1139. https://doi.org/10.2741/3977.

51. Yokota, A., Huo, L., Lan, F., Wu, J., and Huang, G. (2020). The Clinical, Molecular, and Mechanistic Basis of RUNX1 Mutations Identified in Hematological Malignancies. Mol. Cell. *43*, 145–152. https://doi.org/10.14348/molcells.2019.0252.

52. Ahmad, M.H., Hegde, M., Wong, W.J., Mohammadhosseini, M., Garrett, L., Carrascoso, A., Issac, N., Ebert, B., Silva, J.C., Pihan, G., et al. (2023). Runx1-R188Q germline mutation induces inflammation and predisposition to hematologic malignancies in mice. Blood Adv. *7*, 7304–7318. https://doi.org/10.1182/bloodadvances.2023010398.

53. Fan, A.C., Nakauchi, Y., Bai, L., Azizi, A., Nuno, K.A., Zhao, F., Köhnke, T., Karigane, D., Cruz-Hernandez, D., Reinisch, A., et al. (2023). RUNX1 loss renders hematopoietic and leukemic cells dependent on IL-3 and sensitive to JAK inhibition. J. Clin. Invest. *133*, e167053. https://doi.org/10.1172/JCI167053.

54. Bennett, J., and Starczynowski, D.T. (2022). IRAK1 and IRAK4 as emerging therapeutic targets in hematologic malignancies. Curr. Opin. Hematol. *29*, 8–19. https://doi.org/10.1097/MOH.0000000000000693.

55. Hemmati, S., Haque, T., and Gritsman, K. (2017). Inflammatory Signaling Pathways in Preleukemic and Leukemic Stem Cells. Front. Oncol. *7*, 265. https://doi.org/10.3389/fonc.2017.00265.

56. Balandrán, J.C., Lasry, A., and Aifantis, I. (2023). The Role of Inflammation in the Initiation and Progression of Myeloid Neoplasms. Blood Cancer Discov. *4*, 254–266. https://doi.org/10.1158/2643-3230.BCD-22-0176.

57. Bennett, J., Ishikawa, C., Agarwal, P., Yeung, J., Sampson, A., Uible, E., Vick, E., Bolanos, L.C., Hueneman, K., Wunderlich, M., et al. (2023). Paralog-specific signaling by IRAK1/4 maintains MyD88-independent functions in MDS/AML. Blood *142*, 989–1007. https://doi.org/10.1182/blood.2022018718.

58. Barreyro, L., Sampson, A.M., Ishikawa, C., Hueneman, K.M., Choi, K., Pujato, M.A., Chutipongtanate, S., Wyder, M., Haffey, W.D., O'Brien, E., et al. (2022). Blocking UBE2N abrogates oncogenic immune signaling in acute myeloid leukemia. Sci. Transl. Med. *14*, eabb7695. https://doi.org/10.1126/scitranslmed.abb7695.

59. Hodge, C.D., Spyracopoulos, L., and Glover, J.N.M. (2016). Ubc13: the Lys63 ubiquitin chain building machine. Oncotarget *7*, 64471–64504. https://doi.org/10.18632/oncotarget.10948.

60. Wang, T., Pine, A.R., Kotini, A.G., Yuan, H., Zamparo, L., Starczynowski, D.T., Leslie, C., and Papapetrou, E.P. (2021). Sequential CRISPR gene editing in human iPSCs charts the clonal evolution of myeloid leukemia and identifies early disease targets. Cell Stem Cell *28*, 1074–1089.e7. https://doi.org/10.1016/j.stem.2021.01.011.

61. Choi, K., and Ratner, N. (2019). iGEAK: an interactive gene expression analysis kit for seamless workflow using the R/shiny platform. BMC Genom. *20*, 177. https://doi.org/10.1186/s12864-019-5548-x.

62. Subramanian, A., Tamayo, P., Mootha, V.K., Mukherjee, S., Ebert, B.L., Gillette, M.A., Paulovich, A., Pomeroy, S.L., Golub, T.R., Lander, E.S., and Mesirov, J.P. (2005). Gene set enrichment analysis: a knowledge-based approach for interpreting genome-wide expression profiles. Proc. Natl. Acad. Sci. USA *102*, 15545–15550. https://doi.org/10.1073/pnas.0506580102.

63. Koulnis, M., Pop, R., Porpiglia, E., Shearstone, J.R., Hidalgo, D., and Socolovsky, M. (2011). Identification and analysis of mouse erythroid progenitors using the CD71/TER119 flow-cytometric assay. J. Vis. Exp. 2809. https://doi.org/10.3791/2809.

64. Wickham, H. (2009). Ggplot2: Elegant Graphics for Data Analysis. https://doi.org/10.1007/978-0-387-98141-3.

STAR★METHODS

KEY RESOURCES TABLE

REAGENT or RESOURCE	SOURCE	IDENTIFIER
Antibodies		
CD11b-PE-cy7	eBiosciences	25-0112-81
Gr1-eFluor450	eBiosciences	48-5931-82
CD3-PE	eBiosciences	12-0031-83
B220-APC	eBiosciences	17-0452-82
CD45.1	BioLegend	110741
CD45.2	eBiosciences	47-0454-82
lineage biotin panel	eBiosciences	88-7774-75
streptavidin	eBiosciences	47-4317-82
Sca-1-PE	eBiosciences	12-5981-82
c-Kit-APC	eBiosciences	17-1171-81
CD48-FITC	Affymetrix	11-0481-85
CD150-PE-cy7	BioLegend	115914
CD48-APC	Biolegend	103412 Clone HM48-1
CD150 Percp	Biolegend	115922 Clone TC15-12F12.2
cKit-APC-Cy7	eBiosciences	135135, clone ACK2
sAv-eFluor 450	eBiosciences	48-4317-82
CD34-AF700	eBioscience	56-0341-82, clone RAM34
CD16/CD32-BV510	Biolegend	101333, clone 93
Chemicals, peptides, and recombinant proteins		
BrdU	Sigma-Aldrich	B5002
BrdU Flow Kit	BD Biosciences	559619
Methylcellulose	Stemcell Technologies	3434
RNeasy Plus Micro Kit	Qiagen	74034
NSC697923	Selleckchem	S7142
Critical commercial assays		
32-plex mouse cytokine panel	Millipore Sigma	MCYTOMAG-70K
SureSelectXT Mouse All Exon	Agilent Technologies	5190-4641
SPRIworks HT Reagent Kit	Beckman Coulter	B06938
Deposited data		
RUNX1 ChIP seq (multiple data sets)	Sources in Tables S9 and S10	Identifiers in Tables S9 and S10
miR-146a^{KO}/RUNX1^{mut} LSK RNA-seq	This paper	GSE264051, GSE26053
miR-146a^{KO}/RUNX1^{mut} WES	This paper	GSE264052
Experimental models: Organisms/strains		
miR-146a$^{-/-}$ C57BL/6	JAX	016239
C57BL/6	JAX	000664
B6.SJL-Ptprc^a Pepc^b/BoyJ	JAX	002014
Oligonucleotides		
Human Runx1 probes	Taqman	Hs04186042_m1
Murine miR-146a probes	Taqman	hsa-miR-146a

(Continued on next page)

Continued		
REAGENT or RESOURCE	SOURCE	IDENTIFIER
Recombinant DNA		
RUNX1 S291fsX300 (pMYs-IRES-GFP)	Gang Huang	Watanabe-Okochi et al. (ref.[25])
pMYs-IRES-GFP	Addgene	163361
Software and algorithms		
Prism	Graphpad	v10
GSEA	Subramanian et al. (ref.[61])	
Genome Analysis Toolkit	https://www.broadinstitute.org/gatk/	v3.4-46
Burrows Wheeler Aligner	http://bio-bwa.sourceforge.net	BWA v0.7.17
Picard	https://broadinstitute.github.io/picard/	v1.114
Variant Effect Predictor	https://useast.ensembl.org/info/docs/tools/vep/	VEP, v96
Ggplot2	Wickham et al. (ref.[62])	

RESOURCE AVAILABILITY

Lead contact

Further information and requests for reagents can be directed and fulfilled by the lead contact, Daniel Starczynowski (Daniel.Starczynowski@cchmc.org).

Materials availability

This study did not generate new unique reagents.

Cell lines and mouse models used in these studies are publicly available through commercial sources or may be made available from the authors upon written request and material transfer agreement approval. The authors are also glad to share guidance regarding protocols and assays used in these studies upon written request.

Data and code availability

- Bulk RNA-seq and whole exome sequencing data have been deposited at GEO: GSE264053, GSE264051, GSE264052.
- No original code was developed for this study.
- Any additional information required to reanalyze the data reported is available from the lead contact upon request.

METHOD DETAILS

Mouse models

miR-146a^-/- C57BL/6 mice were obtained from Dr. David Baltimore as previously described.[9] All mouse experiments were performed in accordance with the Association for Assessment and Accreditation of Laboratory Animal Care-accredited animal facility of Cincinnati Children's Hospital.

Retroviral vectors, packaging cell lines, and bone marrow transplantation

The RUNX1 S291fsX300 construct inserted between EcoRI/NotI sites in the pMYs-IRES-GFP retroviral vector was obtained from Dr Gang Huang's lab at CCHMC. For retroviral production, 293T cells were co-transfected with the packaging plasmids pCMV-Gag-Pol, pCMV-Eco, and either pMYs-IRES-GFP or pMYs-RUNX1-S291fsX300-IRES-GFP using Fugene6 reagent-based transfection protocol (E2691, Promega). Transfections for retrovirus production were performed in 6 well tissue culture dishes when 293T cells reached at least 80-90% of confluency. 48-hours post-transfection, 293T cell supernatants were collected and filtrated with 0.45um filter. For retroviral transduction, we injected 5-Fluoroacil (80-100 ug/g) into miR146aKO or C57 mice 4 days prior to sacrifice. We harvested the BM cells by flushing the bones and isolated mononuclear cells with histopaque at room temperature. The target cells were resuspended in IMDM containing SCF, TPO and G-CSF (final concentration 100 ng/ml), and seeded in 10cm NTC dishes and culture overnight. Target cells were subjected to two rounds of transduction with retrovirus in two consecutive days. Briefly, transduction was performed in 6-well plates coated with retronectin (20ug/ml) and blocked with 2ml PBS+2%FBS for 30 minutes at room temperature. 2 ml viral supernatant were added to each well and the plate was spun down for 120min at 32C, 800xg. The virus supernatant was removed, and the target cells were added immediately to the plate and incubated overnight. The following day the cells were transduced with a second viral supernatant and polybrene (4 mg/mL; Sigma), and spin-infected with the respective retroviral supernatant for 90min at 32C, 800xg. 24 hours post-transduction, 8×10^4 transduced BM mononuclear cells together with 250,000 wild type whole BM cells were transplanted into lethally irradiated Boy J mice by tail vein injection. For secondary

transplants, 1x10^4 BM and 1x10^6 spleen cells were transplanted into lethally irradiated Boy J recipients along with 2 x10^5 wild-type whole BM by tail vein injection. For serial BM transplantation, 1x10^6 donor-derived BM or spleen cells were isolated from the previous recipients at time of death and transplanted into new lethally irradiated recipients along with fresh 250,000 wild-type whole BM. This process was repeated for two successive rounds. Transplant recipients were periodically bled and analyzed for the presence of GFP positive donor-derived lineage contribution in peripheral blood by flow cytometry.

Cell cycle analysis

BrdU (Sigma-Aldrich) was administered continuously to mice via drinking water (0.5 mg/ml). After 1 week, BrdU incorporation was analyzed using a BrdU Flow Kit (559619, BD Biosciences) according to the manufacture's recommendation.

Colony forming assay

GFP+ LSK CD34-sorted cells (n = 3000 from primary or secondary transplanted mice were plated in 6 well plates with methylcellulose (3434; Stemcell Technologies). Plates were scored with automatic counting on the Stem Cell technologies counter after 7 days in culture. For serial replatings, 5000/ml GFP+ LSK CD34- cells were plated in methyl cellulose for a total of 5 replatings (7, 14, 21, 28, and 35 days).

Hematological analysis

Blood counts were measured with a hemacytometer (HEMAVET).

Flow cytometry

For immunophenotypic analysis of lineage positive cells, PB samples were processed with 1 x RBC lysis buffer, and then incubated with CD11b-PE-cy7 (25-0112-81, eBiosciences), Gr1-eFluor450 (48-5931-82, eBiosciences), CD3-PE (12-0031-83, eBiosciences), and B220-APC (17-0452-82, eBiosciences). To distinguish donor from recipient hematopoietic cells, PB were stained with CD45.1-Brilliant Violet 510 (110741, BioLegend), and CD45.2-APC-eFluor780 (47-0454-82, eBiosciences) or CD45.2- eFluor450 (48-0454-82, eBiosciences). For HSC analysis, BM cells were washed and incubated for 30 minutes with biotin conjugated lineage markers (CD11b, Gr1, Ter119, CD3, B220, mouse hematopoietic lineage biotin panel, [88-7774-75 eBiosciences]), followed by staining with streptavidin eFluor780 (47-4317-82, eBiosciences), Sca-1-PE (12-5981-82, eBiosciences), c-Kit-APC (17-1171-81, eBiosciences), CD48-FITC (11-0481-85, Affymetrix), CD150-PE-cy7 (115914, BioLegend). SLAM-HSC were identified based on expression of Lin$^-$Sca$^-$1$^+$c-Kit$^+$CD150$^+$CD48; multipotent progenitor cells (MPP) were identified based on expression of Lin$^-$cKit$^+$Sca1$^+$CD48$^+$CD150$^-$; short-term hematopoietic stem cells (ST-HSC) were identified based on expression of Lin$^-$cKit$^+$Sca1$^+$CD48$^-$CD150$^-$; long-term hematopoietic stem cells (LT-HSC) were identified based on expression of Lin$^-$cKit$^+$Sca1$^+$CD48$^-$CD150$^+$). CD48-APC (103412 Clone HM48-1, Biolegend), CD150 Percp. Cy5.5 (115922 Clone TC15-12F12.2, Biolegend), cKit-APC-Cy7 (135135, clone ACK2), sAv-eFluor 450 (Streptavidin APC-eFluor® 450, 48-4317-82, eBioscience), CD34-AF700 (56-0341-82, clone RAM34, eBioscience), CD16/CD32-BV510 (101333, clone 93, Biolegend). The identification and analysis of erythroid progenitors was performed as previously described using the CD71/TER119 flow-cytometric assay.[63]

RNA sequencing

Total RNA was extracted from sorted GFP+/lin-/ckit+/Sca+cells using RNeasy Plus Micro Kit (Qiagen). The initial amplification step for all samples was done with the NuGEN Ovation RNA-Seq System v2. The assay was used to amplify RNA samples to create double stranded cDNA. The concentrations were measured using the Qubit dsDNA BR assay. Libraries were then created for all samples using the Illumina protocol (Nextera XT DNA Sample Preparation Kit). The concentrations were measured using the Qubit dsDNA HS assay. The size of the libraries for each sample was measured using the Agilent HS DNA chip. The concentration of the pool was optimized to acquire at least 15-20 million reads per sample. The analysis of RNA sequencing was performed with iGeak.[61] Gene set enrichment analysis (GSEA) was performed as previously described.[62]

Quantitative PCR

cDNA (10-25 ng) extracted from BM aspirates from primary transplanted mice were used to detect the expression of human Runx1 (Taqman probe Hs04186042_m1), and murine miR-146a (hsa-miR-146a Taqman probe) with the 2X Taqman GEA Master mix in a Step One Plus instrument. A GAPDH or U18 taqman probe was utilized for normalization of gene expression.

Cytokine analysis

Peripheral blood was obtained from each mouse in K$_3$ EDTA-coated tubes on ice, then samples were centrifuged for 10 minutes at 2,000 g within 30 minutes at 4°C. After centrifugation, supernatant was immediately transferred to ice cold eppendorf tubes and frozen at -70°C until further use. Samples were thawed on ice, vortexed thoroughly prior to being diluted 1:1 in assay buffer using the mouse cytokines/chemokines magnetic bead panel kit to quantify 32-plex mouse panel (Cat no. MCYTOMAG-70K; Millipore Sigma) following the manufacturer's instructions.

Hematoxylin and eosin staining of BM

Mouse femurs and tibia were dissected and fixed with 10% formalin at room temperature, sectioned and stained with hematoxylin and eosin by the CCHMC pathology core. Imaging performed on the Motic Type 102M Microscope and image capture, and processing was accomplished using Olympus LC Micro Imaging (Olympus) Software and Adobe Photoshop (Adobe).

Peripheral blood, spleen and bone marrow histology

Mouse femurs and tibia were dissected and fixed with 10% formalin at room temperature, sectioned and stained with hematoxylin and eosin or reticulin or anti-cleaved caspase 3 antibody by the CCHMC pathology core. Peripheral blood smears and bone marrow and spleen or liver cytospins were stained with the Hematek 3000 using Hematek Wright-Giemsa (Siemens). Imaging performed on the Motic Type 102M Microscope and image capture, and processing was accomplished using Olympus LC Micro Imaging (Olympus) Software and Adobe Photoshop (Adobe).

Whole exome sequencing

Pooled genomic DNA isolated from FACS sorted BM GFP+/lin-/ckit+/Sca+ cells from WT/vector (n = 3), WT/RUNX1mut (n = 3), miR-146aKO/vector (n = 3), and miR-146aKO/RUNX1mut (n = 3) secondary transplanted mice were submitted to Otogenetics Corporation (Atlanta, GA, USA) for mouse exome capture and sequencing. Briefly, gDNA was subjected to agarose gel and OD ratio tests via Nanodrop to confirm the purity and concentration prior to Bioruptor (Diagenode Inc.) fragmentation. Fragmented gDNAs were tested for size distribution and concentration using an Agilent Tapestation 2200. Illumina libraries were made from qualified fragmented gDNA using SPRIworks HT Reagent Kit (B06938, Beckman Coulter) and the resulting libraries were subjected to exome enrichment using SureSelectXT Mouse All Exon (5190-4641, Agilent Technologies) following the manufacturer's instructions. Enriched libraries were tested for enrichment by qPCR and for size distribution and concentration by an Agilent Bioanalyzer 2100. The samples were then sequenced on an Illumina HiSeq2000/2500 which generated paired-end reads of 100-125 nucleotides with designated average coverage of 30X.

The standard Genome Analysis Toolkit (GATK) pipeline (v3.4-46, https://www.broadinstitute.org/gatk/) was used, with modifications in the "Best Practices" document on their website. Briefly, after applying Illumina's Chastity filter, raw sequenced reads were aligned using the Burrows Wheeler Aligner (BWA v0.7.17, http://bio-bwa.sourceforge.net) against reference mouse genome (GRCm38). For each sample, reads appearing to be PCR artifacts were flagged, reads that overlap known or putative insertions/deletions (INDELs) realigned, then all base quality scores were recalibrated to the empirical error rate from non-polymorphic sites. The GATK HaplotypeCaller module was used to create a gVCF file for each patient sample containing confidence values for every position in the exome (variant and/or reference). A set of variant calls with the GenotypeGVCFs module was generated using every compatible sample sequenced by the sequencing facility to date. The Variant Quality Score Recalibration (VQSR) method was applied to filter variant calls. Finally, variant calls specific to the samples were extracted. Variants marked "PASS" were considered for further analysis. For INDELs, samples were individually preprocessed by realigning reads around putative INDELs using GATK's IndelRealigner tool, marking putative polymerase chain reaction duplicate reads with Picard (v1.114, https://broadinstitute.github.io/picard/) MarkDuplicates tool and by recalibrating base quality scores and calculating Base Alignment Quality scores with GATK's CountCovariates and TableRecalibration tools. After preprocessing, samples were jointly processed with HaplotypeCaller to generate initial variant calls. Variants were then filtered using GATK Variant Quality Score Recalibration. Finally, variants were annotated using Variant Effect Predictor (VEP, v96, https://useast.ensembl.org/info/docs/tools/vep/).

ChIP-sequencing analysis

Collection of public ChIP-seq data from NCBI's GEO database

The objective of this section was to collect and process ChIP-seq experiments targeting the Runx1 protein, performed on stem cells, publicly available in NCBI's Gene Expression Omnibus (GEO) database. The set was curated by following these steps: 1) Programmatic search of public ChIP-seq experiments targeting the Runx1 protein, 2) Programmatic filtering of cell types using the following keywords: "aml|acute| myeloid|lsk|lk|marrow|hematopoietic|leuk", 3) Manual curation to keep experiments that used only stem cells. The final curated sets contained 35 human and 27 mouse ChIP-seq samples targeting the wild type RUNX1 protein in stem cells.

Processing of ChIP-seq data

ChIP-seq reads were downloaded from NCBI's Sequence Read Archive (SRA) database in FASTQ format. The following steps were taken to process the FASTQ data: 1) Quality control of raw reads using FastQC v0.11.9[1], 2) Trimming of adapter sequences or bad quality segments using Trim Galore! v0.6.7[2] and cutadapt v3.5[3], 3) Alignment of trimmed reads to their corresponding reference (human version GRCh38/hg38 and mouse version GRCm39/mm39) with the program HISAT2 version 2.2.1[4], 4) Aligned reads were stripped of duplicate reads with the program sambamba v0.8.2[5], 5) Peaks were called with the program MACS version 2.2.7.1[6], using the narrow peaks mode, 6) Common called peaks from human and mouse, separately, were defined by those present in at least 75% of the samples (20 and 26, respectively) and overlapping by at least 50% of their length (i.e. a ChIP-seq peak is common if it is at least present in 20 out of 27 samples); this was necessary to buffer the uncertainty in observed peaks due to the variable nature of the public samples, with varying laboratory conditions, 7) Common

peaks, in BED format, were converted to a Gene Transfer Format (GTF) to enable fast counting of reads under the peaks with the program featureCounts v2.0.6[7] (Subread package).

The programs Samtools v1.13[8] and Bedtools v2.30.0[9] were used to manipulate BAM and BED file formats, respectively.

QUANTIFICATION AND STATISTICAL ANALYSIS

Differences among multiple groups were assessed by one-way analysis of variance (ANOVA) followed by Tukey's multiple comparison post-test for all possible combinations. Comparison of two group was performed using the Mann-Whitney test or the Student's t test (unpaired, two tailed) when sample size allowed. Unless otherwise specified, results are depicted as the mean $\pm$ standard deviation or standard error of the mean. A normal distribution of data was assessed for data sets >30. D'Agostino and Pearson and Shapiro-Wilk tests were performed to assess data distributions. For Kaplan-Meier analysis, Mantel-Cox test was used. All graphs and analysis were generated using GraphPad Prism software or using the package ggplot2 from R.[64]